Common-Reflection-Surface Stack and Conflicting Dips

Jürgen Mann, Bärbel Traub, and Peter Hubral, Geophysical Institute, University of Karlsruhe, Germany*

Summary

The recently introduced common-reflection-surface (CRS) stack simulates a zero-offset (ZO) section from multi-coverage seismic reflection data for 2-D media without explicit knowledge of the macro-velocity model. The "best" stacking operators are determined by an optimization of the coherency along different test stacking operators in the multi-coverage data. Previous implementations determine only one optimum stacking operator for each ZO sample to be simulated. Consequently, conflicting dips are not taken into account but only the most prominent event contributes to a particular stack sample. This can lead to a lack of coherency of some events in the simulated ZO section. In this work, we show how this limitation can be overcome.

With the term "conflicting dips" we refer to events that would interfere in an actually measured ZO section. In terms of ray theory, multiple ZO rays with different emergence angles contribute to one and the same ZO sample.

The correct simulation of the interference of conflicting events is important for a subsequent post-stack migration, because the lack of coherent energy along less prominent events might cause shadow zones in the migration result.

The pragmatic search strategy of our current CRS stack implementation consists of three one-parametric search steps to determine the stacking operators. In the first step, an automatic CMP stack, conflicting dips can hardly be considered because the respective stacking velocities might be quite similar. However, we observe that conflicting dips can still be detected and separated in the subsequent search steps that are applied to the result of the automatic CMP stack.

We propose an extension of the pragmatic approach to account for conflicting dips. For ZO samples where conflicting dips are detected, we perform an additional one-parametric search. This provides a set of three kinematic wavefield attributes for each of the conflicting events. Stacking along the respective operator for each particular event allows to simulate their interference in the simulated ZO section by means of superposition.

Introduction

The CRS stack method (Müller, 1998, 1999) simulates a ZO section by summing along stacking surfaces in the multi-coverage data. The stacking operator is an approximation of the kinematic reflection response of a curved interface in a laterally inhomogeneous medium. Three kinematic attributes associated with wavefronts of two hypothetical eigenwave experiments are the parameters of the stacking operator. Coherency analyses along various test stacking operators are performed for each particular ZO sample to be simulated. The stacking operator (and its three associated wavefield attributes) yielding the highest coherency is used to perform the actual stack.

Unfortunately, not only one event might contribute to a particular ZO sample, but different events may intersect at the considered ZO location. In case of bow-tie structures, an event will even intersect itself. To properly simulate a ZO section under such conditions, it is no longer sufficient to consider only one stacking operator for each ZO sample, but we have to determine separate stacking operators for each contributing event (or segment of a bow-tie structure). The final stack result can be constructed as a superposition of the contributions of all separate stacking operators.

Figure 1 shows a detail of a simulated ZO section with a bow-tie structure as obtained by the CRS stack without consideration of conflicting dips. The interference of the bow-tie segments is incorrectly simulated. The less prominent bow-tie segment is suppressed at the intersection point and thus broken into two parts.

The lack of coherent energy along the steeper bow-tie segment will cause a shadow zone in a subsequent post-stack migration. Furthermore, no wavefield attributes for this segment are available in the region of intersection. Such gaps in the wavefield attribute sections will cause difficulties in subsequent applications of the attributes.

The modeled ZO section of the synthetic data set used for this example is shown in Figure 2. As expected, the bow-tie segments interfere and the section differs significantly from the ZO section simulated by means of the CRS stack (Figure 1). An ideal CRS stack algorithm should yield the ZO section of Figure 2 rather than that of Figure 1.

Pragmatic search strategy

To be able to follow the pragmatic approach of Müller (1998), let us briefly review some theoretical aspects of the CRS stack: we use a hyperbolic second order representation of the CRS stacking operator which can be derived by means of paraxial ray theory (Schleicher et al., 1993; Tygel et al., 1997). Three independent parameters are used to account for the local properties of the subsurface interfaces: the angle of emergence α of the normal ray and the two radii of curvature R_N and R_{NIP} associated with two hypothetical eigenwave experiments (see, e. g., Mann et al., 1999). The stacking operator reads

$$\begin{aligned} t^2(x_m,h) &= \left(t_0+\frac{2\sin\alpha}{v_0}(x_m-x_0)\right)^2 \\ &+ \frac{2t_0\cos^2\alpha}{v_0}\left(\frac{(x_m-x_0)^2}{R_N}+\frac{h^2}{R_{NIP}}\right), \quad (1) \end{aligned}$$

where the half-offset between source and receiver is denoted by h, and x_m denotes the midpoint between source and receiver. The only required model parameter is the near surface velocity v_0. The respective sample of the ZO trace to be simulated is defined by (t_0, x_0).

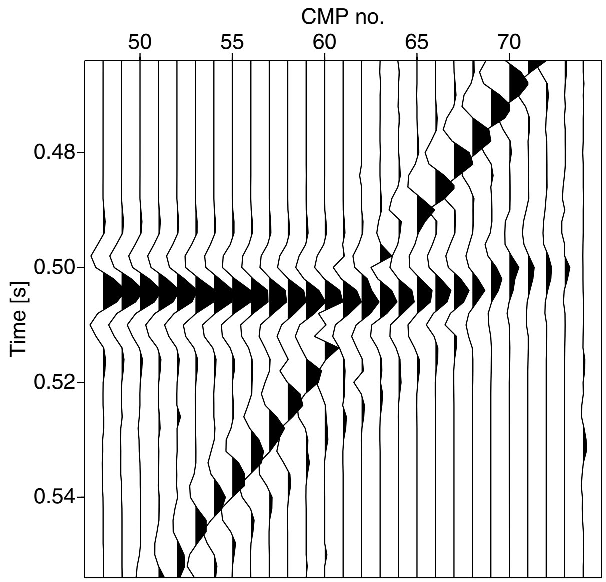

Fig. 1: Detail of a simulated ZO section for a synthetic data set. Conflicting dips are not considered in this application of the CRS stack, therefore the steeper bow-tie segment is broken instead of interfering with the flat bow-tie segment.

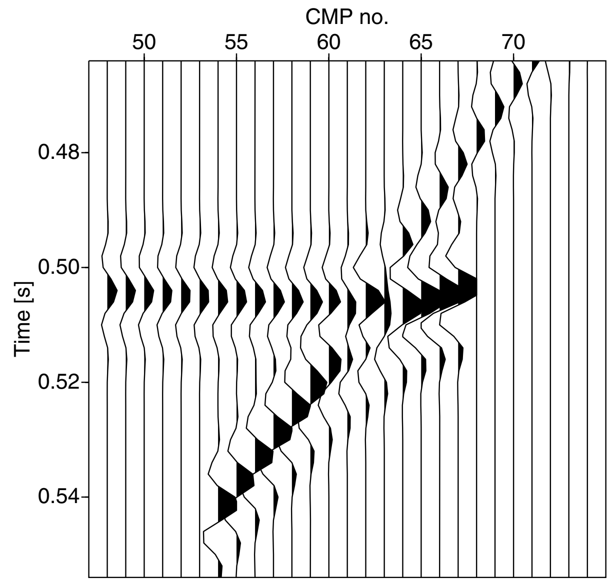

Fig. 2: Detail of the modeled ZO section of the synthetic data set used as input for the result shown in Figure 1. The interference of the intersecting bow-tie segments is clearly visible.

The CRS stack consists of a measure of the coherency of the multi-coverage data along all operators given by Equation (1) for any possible combination of values of α, R_{NIP}, and R_N within a specified test range.

In principle, we have to determine the global maximum and a set of local maxima of the coherency measure in the three-parametric attribute domain. However, even the determination of the global maximum turns out to be too time consuming in a three-parametric search strategy. Therefore, we cannot expect to be able to detect additional local maxima in this way.

Müller (1998) proposed to split the three-parametric problem into three one-parametric searches and an optional three-parametric local optimization as depicted in the simplified flowchart in Figure 3.

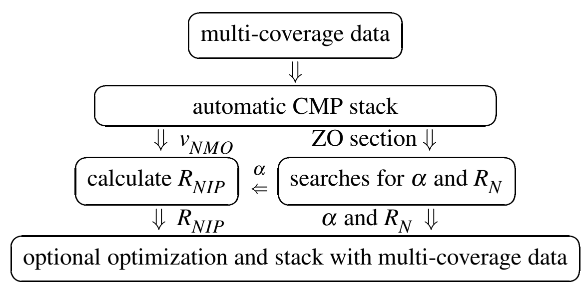

Fig. 3: Simplified flowchart of the pragmatic approach according to Müller (1998).

The first search step of this pragmatic approach is an automatic CMP stack. The search parameter is the stacking velocity v_{NMO} which can be written in terms of the CRS wavefield attributes as

$$v_{NMO}^2 = \frac{2\,v_0\,R_{NIP}}{t_0\,\cos^2\alpha}\,. \tag{2}$$

The next two search steps are applied to the CMP stacked section. The search parameters are α and R_N. The former is then used to calculate R_{NIP} by means of formula (2).

Conflicting dips

This three-step strategy has to be modified if conflicting dips are to be correctly taken into account. Unfortunately, in spite of the angle-dependence of v_{NMO}, we cannot rely on the first step to separate events with different emergence angles because the associated stacking velocities might be similar or even identical. Furthermore, the sign of the emergence angle α cannot be determined by means of Equation (2).

However, it is possible to detect events with different emergence angles in the second step in the CMP stacked section, although these have not been correctly taken into account by the preceeding automatic CMP stack. This is indicated by Figure 4, which was obtained from a real data example. For a given point in the ZO section to be simulated the coherency values are plotted versus the tested emergence angles. We observe three distinct local maxima which are potential candidates for conflicting dips.

We have computed the “angle spectrum” depicted in Figure 4 for a deep-offshore data set. At the considered ZO location, two diffraction patterns (at $\alpha \approx -30°$ and $\alpha \approx 25°$, respectively) and a weak reflection event (at $\alpha \approx 12°$) intersect each other.

Due to the above observations, the three-step approach can be

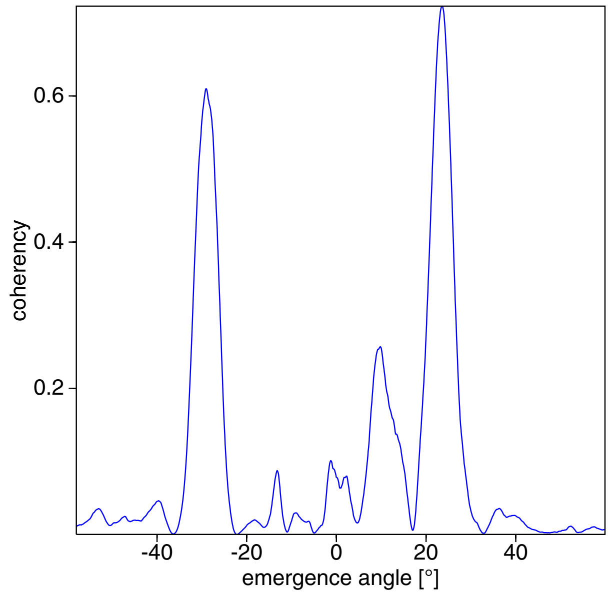

Fig. 4: Coherency measure plotted versus the tested angles of emergence of the normal ray. Distinct local maxima can be observed, although conflicting dips have not been considered in the preceeding step.

easily extended such as to detect conflicting events with different emergence angles. However, the calculation of R_{NIP} from α and v_{NMO} according to Equation (2) is no longer possible, because, in general, we will detect more than one angle of emergence but only one value for the stacking velocity v_{NMO}. Consequently, the approach has to be adapted to account for this fact. An additional search procedure for each radius of curvature $R_{NIP}^{(i)}$ corresponding to each conflicting dip $\alpha^{(i)}$ becomes necessary.

Unfortunately, $R_{NIP}^{(i)}$ can be determined neither in the CMP stacked section nor in the original CMP gathers. According to the stacking operator (1), $R_{NIP}^{(i)}$ does not influence in the ZO section $(h = 0)$, and in the CMP gather $(x_m = x_0)$, $R_{NIP}^{(i)}$ and $\alpha^{(i)}$ cannot be separated. To solve this problem, we propose to perform the additional search for $R_{NIP}^{(i)}$ in the entire multi-coverage data set. A simplified flowchart of this strategy is depicted in Figure 5.

If only one event for a particular ZO sample is detected, we can still use the pragmatic scheme (Figure 3) without the explicit search for $R_{NIP}^{(i)}$. Otherwise, the automatic CMP stack only serves to provide a simulated ZO section in which $\alpha^{(i)}$ and $R_N^{(i)}$ can be easily detected, whereas the stacking velocity is not explicitly used anymore.

Conclusions

The pragmatic approach of Müller (1998) to perform a ZO simulation by means of the CRS stack method can be adapted to also account for the conflicting dip problem. An additional one-parametric search is required to resolve ambiguities introduced by different events contributing to one and the same ZO sample to be simulated.

The consideration of conflicting dips is necessary to obtain a more physical simulation of a ZO section: the simulated interference of intersecting events is closer to the result of an actual ZO measurement.

In addition to the improved simulated ZO section, the adapted CRS stack strategy provides three kinematic wavefield attributes for each particular event, even if it intersects one or more other events (or its own bow-tie segments). Subsequent applications of these wavefield attributes (e. g., an inversion of the macro-velocity model, calculation of Fresnel zones etc.) benefit from this fact, because otherwise the wavefield attributes in the gaps between "broken" event segments would have to be interpolated.

multi-coverage data

$\Downarrow$

automatic CMP stack

$\Downarrow$ ZO section

searches for $\alpha^{(i)}$ and $R_N^{(i)}$

$\Downarrow$ $\alpha^{(i)}$ and $R_N^{(i)}$

search for $R_{NIP}^{(i)}$ in multi-coverage data

$\Downarrow$ $\alpha^{(i)}$, $R_{NIP}^{(i)}$, and ${R_N}^{(i)}$

optional optimization and stack in multi-coverage data

Fig. 5: Simplified flowchart of the adapted search strategy. The index i denotes the different events detected for one and the same ZO sample.

Acknowledgments

This work was kindly supported by the sponsors of the *Wave Inversion Technology Consortium*, Karlsruhe, Germany and the *Federal Institute for Geosciences and Natural Resources*, Hannover, Germany.

References

Mann, J., Jäger, R., Müller, T., Höcht, G., and Hubral, P., 1999, Common-reflection-surface stack - a real data example: J. Appl. Geoph., **42**, no. 3,4, 301–318.

Müller, T., 1998, Common Reflection Surface Stack versus NMO/STACK and NMO/DMO/STACK: 60th Mtg. Eur. Assoc. Expl. Geophys., Extended Abstracts.

Müller, T., 1999, The common reflection surface stack - seismic imaging without explicit knowledge of the velocity model: Der Andere Verlag, Bad Iburg.

Schleicher, J., Tygel, M., and Hubral, P., 1993, Parabolic and hyperbolic paraxial two-point traveltimes in 3D media: Geophys. Prosp., **41**, no. 4, 459–513.

Tygel, M., Müller, T., Hubral, P., and Schleicher, J., 1997, Eigenwave based multiparameter traveltime expansions: 67th Annual Internat. Mtg., Soc. Expl. Geophys., Expanded Abstracts, 1770–1773.